ACTIVE VIBRATION ISOLATION DESIGN FOR A PHOTOLITHOGRAPHIC STEPPER

Pradeep Subrahmanyan,* Mark Williams, David Trumpert**

ABSTRACT

This paper discusses the design and implementation of a six axis active/passive vibration isolation system on a photolithographic stepper. Passive isolation is used to provide good isolation at high frequencies and to support the static weight of the stepper. Active isolation is used to provide the dynamic control forces to reject external disturbances. The active system has the capability to reject both seismic disturbances and reaction forces resulting from wafer stage motions.

A description of the system hardware is presented followed by dynamic system modeling and details of the control approach used. A series of coordinate transformations to implement simple control laws are derived. Active control is established over more than two decades around the mount resonant frequency and about 30-40 dB attenuation of disturbances achieved. Experimental results verify the performance of the system. These results illustrate the effectiveness of the system at rejecting disturbances originating from both seismic sources and from the motion of the wafer stage.

INTRODUCTION

The performance of a photolithographic stepper is typically measured in terms of its throughput and overlay[1]. Surrounding environmental conditions can degrade stepper performance, and machine vibrations are a significant contributor to the total error. In this paper we present an integrated six degree of freedom active seismic isolation system with the additional capability to compensate for payload reaction forces (Williams, Subrahmanyan and Trumper, 1997). The system comprises both active and passive el-

[1]The throughput of a stepper is generally defined in wafers per hour and the overlay is a measure of a machine's ability to place successive exposure layers in the same position.

*Rm. 35-030, Massachusetts Institute of Technology, 77 Massachusetts Avenue, Cambridge, MA 02139, USA, pks@mit.edu.

**Integrated Solutions Inc., 836 North Street, Bldg. 5, Tewksbury, MA 01876, USA, williams@mail.insol.com.

†Rm. 35-014, Massachusetts Institute of Technology, 77 Massachusetts Avenue, Cambridge, MA, USA, 02139 trumper@mit.edu.

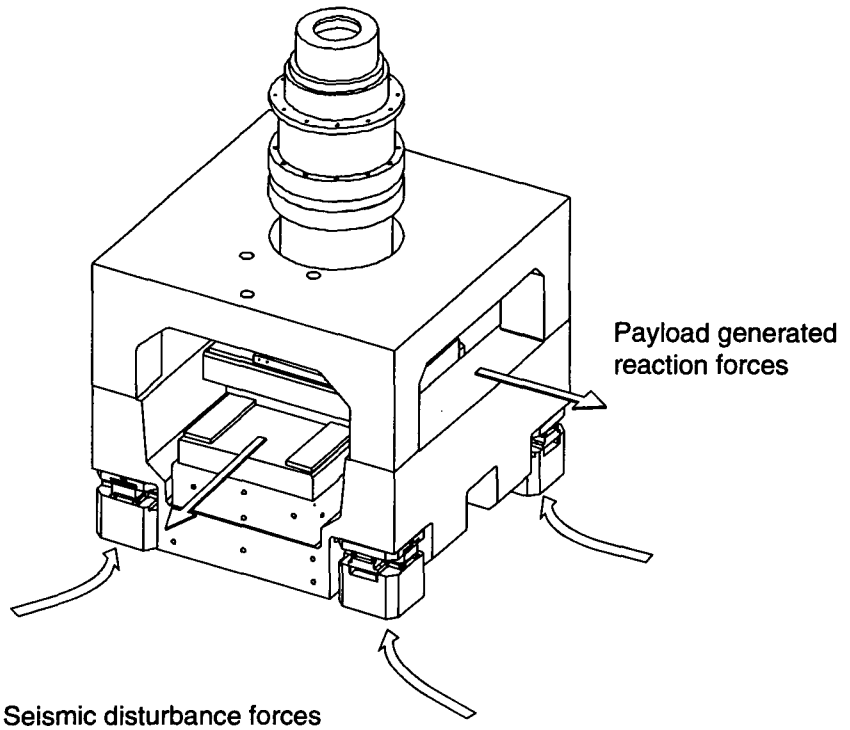

Figure 1: Schematic of prototype stepper showing disturbance mechanisms

ements to allow the isolation or control of disturbance forces in a band which extends from frequencies of about 0.1 Hz to 50 Hz, providing about three decades of isolation. The isolation system is implemented on a prototype stepper shown in Figure 1. The two distinct sources of disturbances are also shown in Figure 1. The vibrations induced by stage motions are deterministic in nature and are readily compensated for with feedforward control techniques. During wafer exposure, the primary source of vibration is from seismic level base disturbances. These vibrations are usually stochastic and broadband in nature.

In summary, this paper will present the mechanical design and the control approach implemented on a prototype stepper. Both ground vibration transmissibility data and transient response of the system during stage accelerations will be presented. As lithography tools improve in performance, and the industry moves toward very high throughput platforms, these precision isolation and disturbance rejection issues become increasingly more critical.

MECHANICAL DESCRIPTION

The isolation system consists of passive elastomeric mounts that support the mass of the system and also attenuate seismic disturbances above approximately 20 Hz. The shape of the elastomer is chosen such that the longitudinal and lateral stiffness match. Additionally, damping in the elastomer mounts is hysteretic, so an increase in damping ratio does not lead to degradation of performance at higher frequencies. In order to actively

control disturbance forces at frequencies below the elastomer capabilities, the system utilizes sixteen variable reluctance tractive type force actuators to control acceleration in six degrees of freedom. These actuators are chosen for their high specific force and relatively large stroke. The system acceleration is sensed and fed back to a digital controller by six seismic accelerometers. These accelerometers are selected based on their high signal to noise ratio even at very low frequencies. Three of the accelerometers have a vertical orientation and sense $\ddot{Z}, \ddot{\theta}_x$, and $\ddot{\theta}_y$. The remaining three accelerometers are oriented horizontally and sense $\ddot{X}, \ddot{Y}$, and $\ddot{\theta}_z$. The isolation system actuators are contained in the four

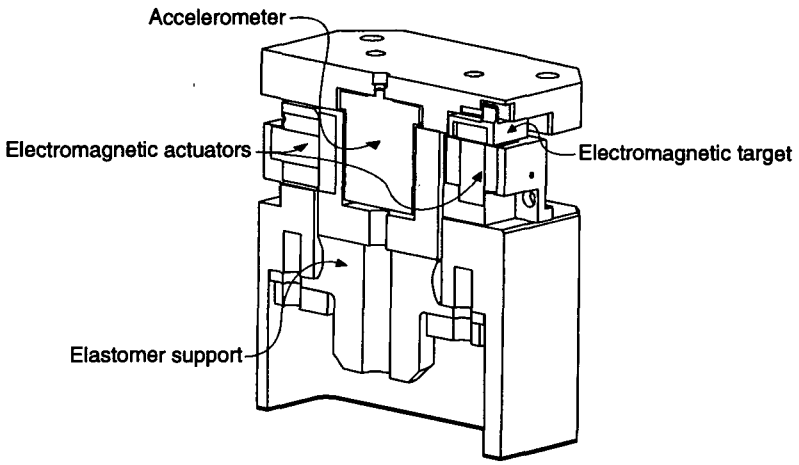

Figure 2: Cutaway view of one leg of the system

supports at each corner of the stepper base. A more desirable arrangement is to use three legs separated by 120° and located closer to the plane that passes through the system center of gravity. This more desirable geometry results in an isolation system that has decoupled rotational and translational natural modes. However, the four support configuration is used to allow a direct substitution for the passive isolation system currently used on production steppers. Figure 2 is a cutaway view of one of the isolation legs. In this figure, the placement of the elastomer, accelerometer, and actuators can be seen. As seen in Figure 3, the actuators are arranged such that the X and Y force pairs are distributed amongst the four legs and the four Z bi- directional pairs are each located on a single leg. The eight pairs of actuators are symmetrically placed and are sized large enough to compensate for a 1-g acceleration of a 30 kg mass (300 N).

The wafer stage consists of two stacked single degree of freedom air bearing stages which transport a magnetically levitated six degree of freedom small motion stage. The stiffness of the air bearings is high enough that a rigid connection can be assumed in all the axes other than the axis of motion. The design and implementation of the Mag-Lev fine stage has been described in (Williams et al., 1997).

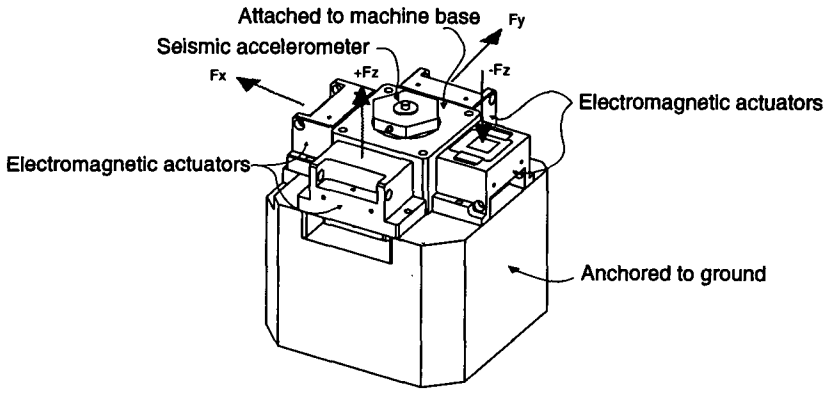

Figure 3: Forces provided at each leg location

MODELING

In this section, we derive the equations governing the motion of the rigid body. The stepper is modeled as a rigid body on elastic mounts modeled as springs and dampers[2] as shown in Figure 4. This rigid body assumption is valid in this case since the lowest elastic mode is above the active control bandwidth.

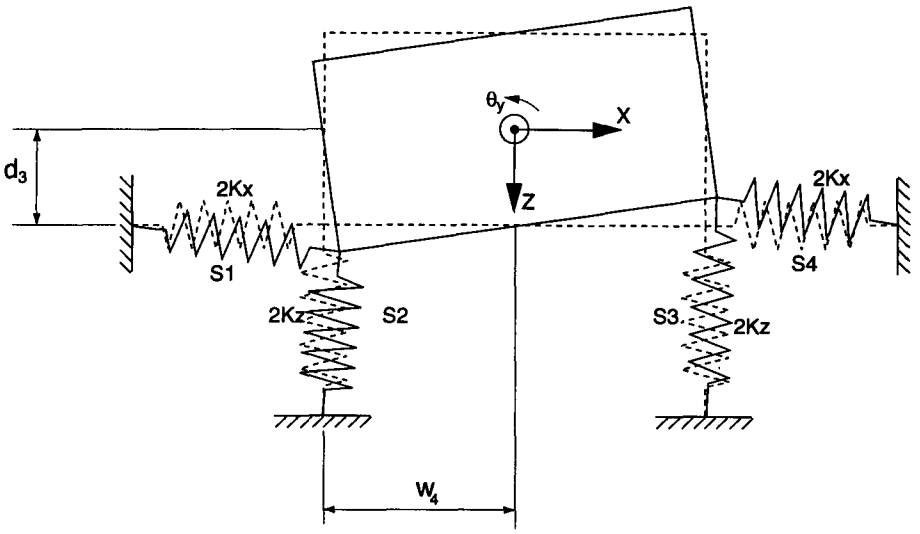

Figure 4: Displaced three degree of freedom model

Because of the stepper mounting arrangement there is significant coupling between X and θ_y motions and Y and θ_x motions. However, due to symmetry, the Z and θ_z degrees of freedom are largely decoupled. We use the three degree of freedom system shown in Figure 4 to model the stepper in both the XZ and YZ planes. In the derivation, only the principle moments of inertia are used and the products of inertia are ignored since

[2]We assume a damping term to enter the equations of motion exactly like the stiffness terms (since the dampers are in parallel with the springs, although not shown in the figures).

the magnitudes are insignificant in comparison. Besides, only small displacements are considered and hence both the equations and geometric transformations that follow are linear. The governing equations are listed below :

$$\begin{aligned}
M\ddot{x} + 4C_x\dot{x} + 4K_x x + 4d_3C_x\dot{\theta}_y + 4d_3K_x\theta_y &= F_x \\
M\ddot{y} + 4C_x\dot{y} + 4K_x y - 4d_3C_x\dot{\theta}_x - 4d_3K_x\theta_x &= F_y \\
M\ddot{z} + 4C_z\dot{z} + 4K_z z &= F_z \\
I_{xx}\ddot{\theta}_x - 4d_3C_x\dot{y} - 4d_3K_x y + 4\left(d_3^2C_x + l_4^2C_z\right)\dot{\theta}_x + 4\left(d_3^2K_x + l_4^2K_z\right)\theta_x &= \tau_x \\
I_{yy}\ddot{\theta}_y + 4d_3C_x\dot{x} + 4d_3K_x x + 4\left(d_3^2C_x + w_4^2C_z\right)\dot{\theta}_y + 4\left(d_3^2K_x + w_4^2K_z\right)\theta_y &= \tau_y \\
I_{zz}\ddot{\theta}_z + 4\left(w_4^2 + l_4^2\right)C_x\dot{\theta}_z + 4\left(w_4^2 + l_4^2\right)K_x\theta_z &= \tau_z
\end{aligned} \tag{1}$$

The inertial parameters of the stepper are in standard notation. K_z is the longitudinal (Z-direction) stiffness of the mount; K_x is its lateral stiffness with C_z and C_x being the corresponding damping terms. w_4, l_4 and d_3 are the distances of the mounts from the centroidal coordinate frame of the stepper in the X, Y and Z directions, respectively.

There is significant coupling between the rigid body accelerations and the control forces as shown by the governing equations. This leads us to pursue multi-variable control design techniques. The simplest approach to multi-variable control is through decoupling transformations. This approach involves identifying the natural modes of the system and performing control in these modal coordinates. To preface a control implementation we first establish a set of decoupling coordinate transformations.

COORDINATE FRAMES

There are four relevant coordinate frames for the isolation system. They are as follows :

- Sensor coordinate frame
- Stepper (Cartesian) coordinate frame
- Control (Modal) coordinate frame
- Actuator coordinate frame

One can switch between coordinate frames using the geometric transformations developed below. This is possible since the stepper is considered a rigid body and the transformations are only a function of the stepper geometry.

The accelerometers measure linear acceleration at their mounting locations, *i.e.*, the sensor coordinate frame. These point-wise accelerations are transformed to rigid body accelerations about the centroidal Cartesian coordinate frame. This is accomplished by means of a linear transformation given by

$$\ddot{\mathbf{x}} = \mathbf{A}_{\mathbf{accn}}\ddot{\mathbf{x}}_{\mathbf{sensor}} \tag{2}$$

where $\ddot{\mathbf{x}}$ is the acceleration vector expressed in the Cartesian coordinate frame and $\ddot{\mathbf{x}}_{\mathbf{sensor}}$ is the acceleration vector expressed in the sensor coordinate frame. The matrix $\mathbf{A}_{\mathbf{accn}}$ is a function of sensor location.

Similarly, actuators apply control forces at various discrete locations on the stepper structure. The control forces and torques which can originate in either the Cartesian or modal coordinate frame need to be transformed to the physically realizable actuator coordinate frame. This is accomplished by the linear transformation given as

$$\mathbf{F_{actuator}} = \mathbf{A_{force}}\mathbf{F} \tag{3}$$

where $\mathbf{F}$ is the force vector expressed in the Cartesian coordinate frame and $\mathbf{F_{actuator}}$ is the force vector expressed in the actuator coordinate frame. Again, the matrix $\mathbf{A_{force}}$ is a function of actuator location.

As will be shown, control is performed in the modal coordinate frame since the equations of motion of the stepper are decoupled in this coordinate frame. To establish these decoupling transformations, we rewrite the equations of motion in concise matrix notation as

$$\mathbf{M}\ddot{\mathbf{x}} + \mathbf{C}\dot{\mathbf{x}} + \mathbf{K}\mathbf{x} = \mathbf{F} \tag{4}$$

We first look for responses of the form $\mathbf{x} = \mathbf{X}\sin(\omega t)$ where all the displacements of the system occur at the same frequency and differ only in amplitudes as given by the vector $\mathbf{X}$. Such a mode of motion is called a natural mode (Meirovitch, 1986). In the absence of any input forces and damping, the natural modes are given by

$$\Rightarrow (\mathbf{M}^{-1}\mathbf{K})\mathbf{X} = \omega^2\mathbf{X} \tag{5}$$

which is the standard eigenvalue problem with eigenvalues, $\lambda_i = \omega_i^2$ and eigenvectors $\mathbf{v}_i$ where the subscripts correspond to the i^{th} natural mode. The modal matrix $\mathbf{V}$ is then obtained by setting the columns to the eigenvectors $\mathbf{v}_i$. With independent eigenvectors, we can now diagonalize the equations of motion using the following transformation

$$\begin{aligned} \mathbf{x} &= \mathbf{V}\eta \\ \Rightarrow \eta &= \mathbf{V}^{-1}\mathbf{x} \end{aligned} \tag{6}$$

Expressing the equations of motion in terms of the modal coordinates η and premultiplying by V^T, we obtain the modal equations of motion

$$\mathbf{V}^T\mathbf{M}\mathbf{V}\ddot{\eta} + \mathbf{V}^T\mathbf{C}\mathbf{V}\dot{\eta} + \mathbf{V}^T\mathbf{K}\mathbf{V}\eta = \mathbf{V}^T\mathbf{F} \tag{7}$$

$$\Rightarrow \mathbf{M_m}\ddot{\eta} + \mathbf{C_m}\dot{\eta} + \mathbf{K_m}\eta = \mathbf{F_m} \tag{8}$$

where we have defined the following modal matrices :

$$\begin{aligned} \mathbf{M_m} &= \mathbf{V}^T\mathbf{M}\mathbf{V} \\ \mathbf{C_m} &= \mathbf{V}^T\mathbf{C}\mathbf{V} \\ \mathbf{K_m} &= \mathbf{V}^T\mathbf{K}\mathbf{V} \\ \mathbf{F_m} &= \mathbf{V}^T\mathbf{F} \end{aligned} \tag{9}$$

We further note that the eigenvectors are also orthogonal with respect to the mass and stiffness matrices thus making the modal mass and stiffness matrices $\mathbf{M_m}$ and $\mathbf{K_m}$ diagonal. However, the modal damping matrix is not diagonal since the eigenvectors are not

guaranteed to be orthogonal to it. We make one further assumption and consider only the diagonal entries of the modal damping matrix. This is similar to modal damping where a damping ratio is assigned to each mode.

Equation 8 then is a set of six decoupled second-order equations for which single-input single-output controllers can readily be implemented. Control outputs are then computed to give the modal force vector $\mathbf{F_m}$ which is related to the Cartesian force vector through the modal transformations given by equation 9. The Cartesian coordinate frame forces are then converted into the actuator frame. These transformations can be cascaded to relate the modal coordinate frame directly to the actuator coordinate frame.

$$\mathbf{F_{actuator}} = \mathbf{T_{fm}}\mathbf{F_m} \tag{10}$$

where $\mathbf{F_m}$ is the force vector in the modal coordinate frame and $\mathbf{F_{actuator}}$ is the force vector in the actuator coordinate frame. The transformation matrix $\mathbf{T_{fm}}$ is given by

$$\mathbf{T_{fm}} = \mathbf{A_{force}}\mathbf{V}^{-T} \tag{11}$$

Similarly the sensor coordinate frame can be related to the modal coordinate frame so that the feedback acceleration signals are expressed in the modal coordinate frame. We then arrive at the following equation

$$\ddot{\eta} = \mathbf{T_{sm}}\ddot{\mathbf{x}}_{\mathbf{sensor}} \tag{12}$$

where $\ddot{\eta}$ is the acceleration vector expressed in the modal coordinate frame and $\ddot{\mathbf{x}}_{\mathbf{sensor}}$ is the acceleration vector expressed in the sensor coordinate frame. The transformation matrix $\mathbf{T_{sm}}$ is given by

$$\mathbf{T_{sm}} = \mathbf{V}^{-1}\mathbf{A_{accn}} \tag{13}$$

We have the six decoupled equations of motion and the means to relate these decoupled accelerations and control forces to the measured accelerations and applied control forces. We are now in a position to derive the control law in the next section.

CONTROL

Passive isolation is very effective for frequencies above the active control bandwidth of 50 Hz. In fact active control at higher bandwidths can cause the performance to deteriorate due to increased noise sensitivity at these frequencies. We also note that the only coupling between the stage and the stepper base is that due to the stage control forces. This coupling can be accounted for by feedforward techniques discussed in the next section. This allows us to decouple the controller design for the isolation system from that of the stage, thereby permitting the development of less complex control strategies. Since the stepper can be modeled as a decoupled system in modal coordinates using the techniques described in the previous section, the control design is essentially that for a simple mass/spring/damper system. A loop-shaping control strategy is adopted to provide acceptable lower and upper bandwidths and reasonable phase margin at the crossover frequencies (Franklin, Powell and Workman, 1990) for the decoupled SISO systems. The

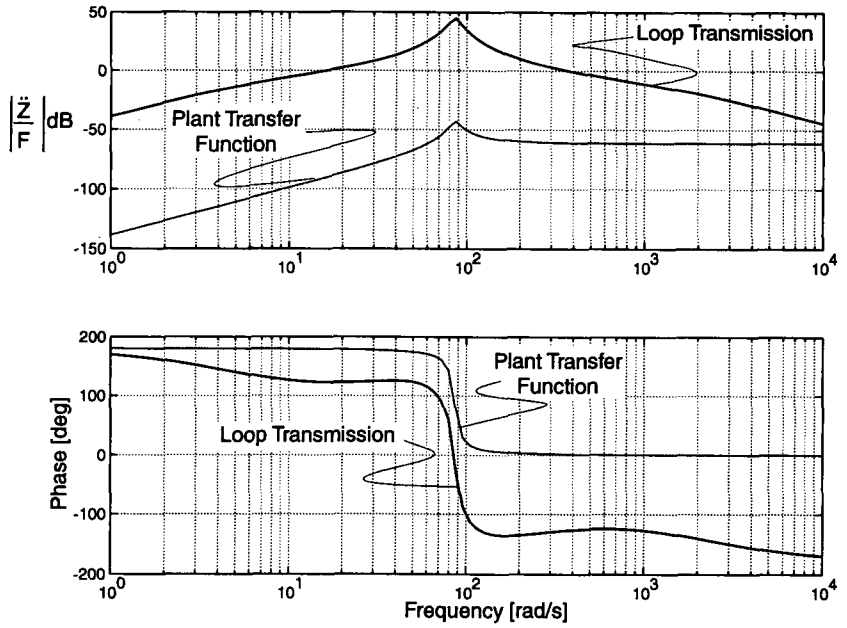

Figure 5: Typical loop transmission for a mass/spring/damper system

active control region is denoted by the region in which the loop transmission is greater than unity (0 dB). A typical loop transmission is shown in Figure 5.

The effect of active control is shown in a theoretical transmissibility plot in Figure 6. Here, the transmissibility of the active mount is compared with that of the passive mount. This shows the effect of suppressing the resonance of the passive system in addition to attenuating disturbances over the control bandwidth. The upper and lower bandwidths and the gain are set by the control bandwidth requirement, the noise sensitivity requirement, allowable control effort, and the dynamic characteristics of the plant itself.

FEEDFORWARD CONTROL

The feedforward part of the control adds control forces to compensate for the reaction forces caused due to stage accelerations. The stage reaction forces are transformed into the modal coordinate system using another linear transformation and added to the feedback control forces. The transformation that relates the isolation system's control forces to the stage forces (which are computed according to a different control law) is given by

$$\mathbf{F_{ffmodal}} = \mathbf{V^T A_{ff} F_{stage}} \tag{14}$$

Here, $\mathbf{F_{stage}}$ is a vector of the stage forces, $\mathbf{A_{ff}}$ is a geometric matrix which is a function of the instantaneous position of the linear motor control forces in the stepper coordinate frame, $\mathbf{V}$ is the modal matrix, and $\mathbf{F_{ffmodal}}$ is the vector of feedforward forces added to the vector of feedback forces. It should be noted that both the feedforward and feedback control forces are expressed in the same coordinate system, *i.e.*, the modal coordinate system.

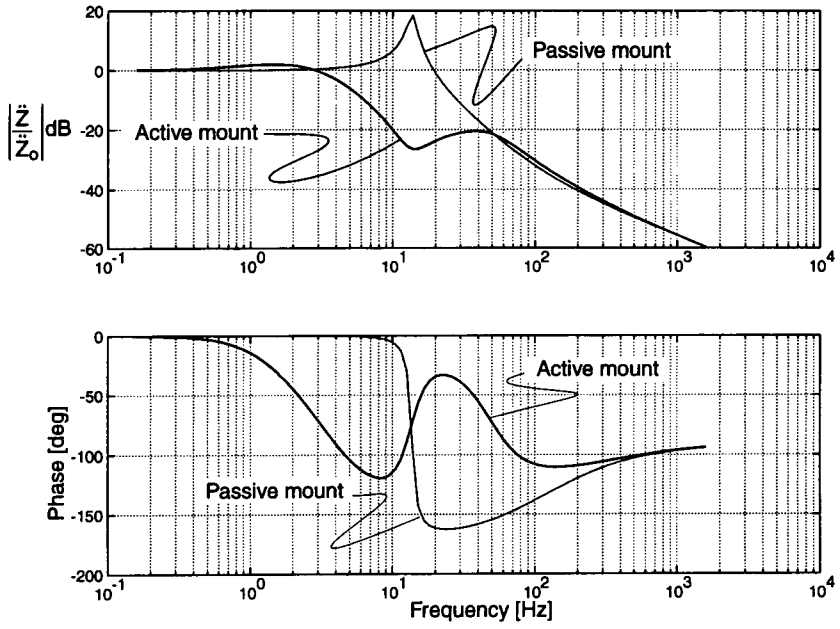

Figure 6: Transmissibility plots for active/passive mounts

IMPLEMENTATION

The control is implemented on a Texas Instruments C40 DSP with a sampling rate of 5 KHz. The implementation of the control scheme developed so far is illustrated in Figure 7. The sampled accelerations are passed through a digital high-pass filter to remove any D.C. bias in the signals. The modal accelerations (computed using the transformations given in equation 12) are used in the computation of the modal control forces according to the feedback control law described earlier. The stage positions and control forces are then

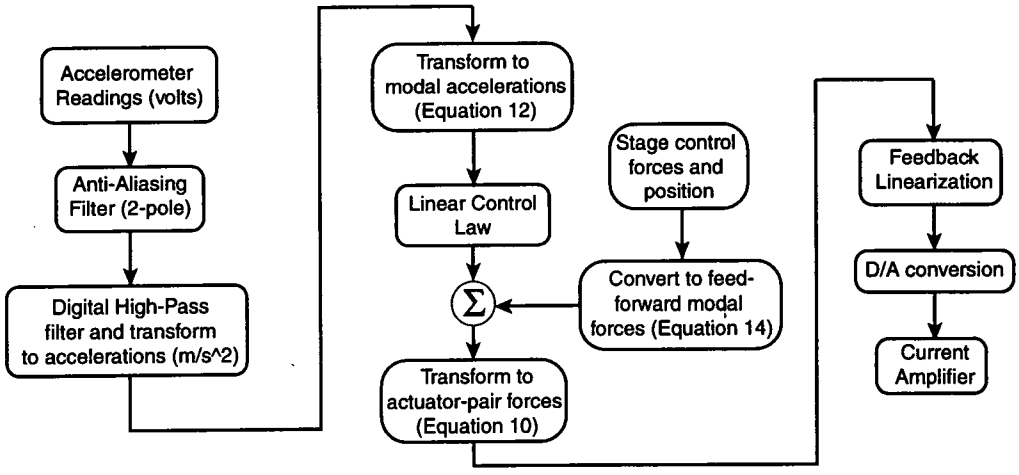

Figure 7: Implementation of control scheme

used to compute the feedforward forces using the transformation given in equation 14. These are added to the feedback forces to give the overall control forces. The individual

actuator forces are then computed according to the transformations given in equation 10. The control currents for the individual actuators are then computed using a feedback linearization law (Trumper, Olsen and Subrahmanyan, 1997). The feedback linearization law assumes constant gaps which are set at startup. The constant air gap assumption is valid since the motions of the stepper are very small. The control voltages corresponding to the control currents are written to the DACs which are connected to the current amplifiers that power the individual actuators.

EXPERIMENTAL RESULTS

Two sets of experiments were done to ascertain the performance of the active vibration isolation system. The first is a seismic transmissibility test in the Z direction. Floor

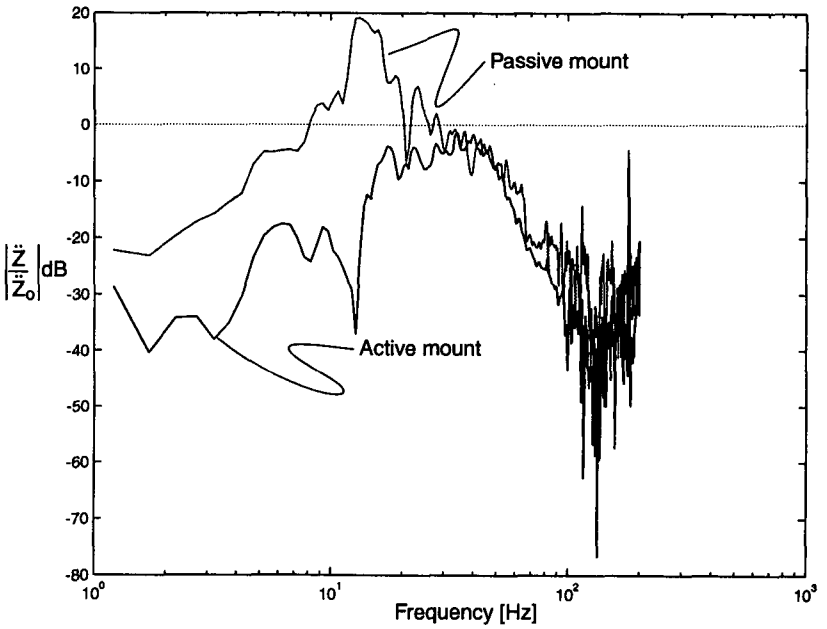

Figure 8: Z axis Transmissibility

vibrations are measured using a seismic accelerometer and the vibrations of the stepper are computed using the transformations given in equation 2. The experimentally measured active-on/active-off transmissibility is plotted in Figure 8. The passive transmissibility curve clearly shows the resonant peak due to the lightly damped passive mounts. The active transmissibility curve shows a clear attenuation of approximately 30 dB at the resonant peak.

A second experiment was performed to quantify the transient performance of the isolation system during stage motions. As shown in Figure 9 a typical step of 20 mm is taken in the X direction with a stage acceleration of 3 m/sec^2 (0.3 g). The theoretical acceleration of the stepper (stage acceleration divided by the mass ratio of stepper/stage) is plotted with the measured acceleration. With the active system off, the stepper oscillates at the natural frequency of the isolation mount due to the inertial forces of the accelerating stage. With the active system on, the oscillation is arrested almost immediately. The

spikes correspond to the acceleration profile (trapezoidal velocity) of the stage. This is to be expected since the effectiveness of feedforward control is a function of the accuracy of the dynamic model.

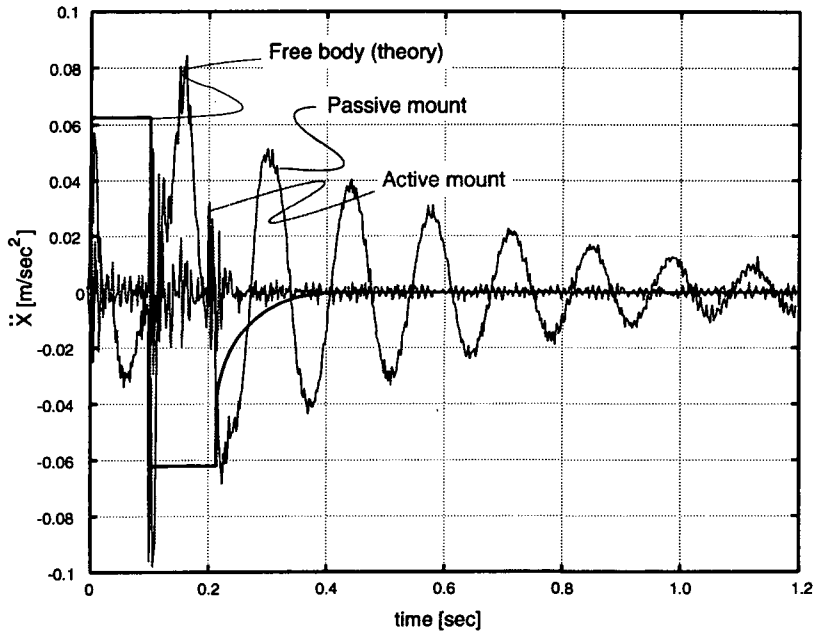

Figure 9: Isolation performance during stage motions

CONCLUSIONS

This paper describes the design of an active isolation system for a photolithographic stepper and demonstrates the application of modal techniques to convert the MIMO isolation problem of the stepper into a system of decoupled second order systems. The problem of isolation design for second order systems is very well understood and hence can be applied to the systems in the modal domain. Experimental results are presented to demonstrate the significant gains in settling time obtained by the use of active/passive vibration isolation strategies.

REFERENCES

Franklin, G.F., Powell, J.D., Workman, M.L., 1990, "Digital Control of Dynamic Systems - 2^{nd} edition", Addison-Wesley, Reading.

Meirovitch, L., 1986, "Elements of Vibration Analysis - 2^{nd} edition", McGraw Hill, New York.

Trumper, D.L., Olsen, S.M., Subrahmanyan, P.K., 1997, "Linearizing Control of Magnetic Suspension Systems", *IEEE Transactions on Control Systems Technology*, Vol. 5, Number 4, pp 427-438.

Williams, M.,Faill, P., et.al., 1997, "Six Degree of Freedom Mag-Lev Stage Development", Proceedings of the SPIE Conference, Vol. 3051.

Williams, M., Subrahmanyan, P., Trumper, D.L., 1997, "Six Axis Active Vibration Isolation and Payload Reaction Force Compensation System", Proceedings of the 12^{th} Annual ASPE Meeting, Norfolk, VA, pp 494-497.

SYSTEM MATRICES

Some of the system matrices are listed below. Note that the matrices $\mathbf{A_{accn}}$ and $\mathbf{A_{force}}$ are constant while $\mathbf{A_{ff}}$ is a function of y_{fcx} (the coarse X-stage position in the Y-direction).

$$\mathbf{A_{accn}} = \begin{pmatrix} 0.5000 & -0.5000 & 0 & -0.4525 & 0.4525 & 0 \\ 0.4908 & 0.4908 & -1.0000 & -0.4438 & 0 & 0.4438 \\ 0 & 0 & 0 & -0.0349 & -0.4651 & -0.5000 \\ 0 & 0 & 0 & -1.3483 & 0 & 1.3483 \\ 0 & 0 & 0 & 1.3747 & -1.3747 & 0 \\ -1.3483 & -1.3483 & 0 & 0 & 0 & 0 \end{pmatrix} \tag{15}$$

$$\mathbf{A_{force}} = \begin{pmatrix} -0.5000 & 0.0175 & 0 & 0 & 0 & 0.6872 \\ -0.5000 & -0.0175 & 0 & 0 & 0 & -0.6872 \\ 0 & -0.5171 & 0 & 0 & 0 & -0.6740 \\ 0 & -0.4829 & 0 & 0 & 0 & 0.6740 \\ 0.2315 & 0.2277 & 0.2340 & 0.6182 & -0.6285 & 0 \\ 0.2315 & -0.2277 & 0.2340 & -0.6182 & -0.6285 & 0 \\ -0.2315 & -0.2277 & 0.2660 & -0.6182 & 0.6285 & 0 \\ -0.2315 & 0.2277 & 0.2660 & 0.6182 & 0.6285 & 0 \end{pmatrix} \tag{16}$$

$$\mathbf{A_{ff}} = \begin{pmatrix} 1 & 0 \\ 0 & 1 \\ 0 & 0 \\ 0 & -0.3556 \\ 0.254 & 0 \\ -y_{fcx} & 0.025 \end{pmatrix} \tag{17}$$